Contents lists available at ScienceDirect

Agricultural Water Management

journal homepage: www.elsevier.com/locate/agwat

Mapping soil moisture across an irrigated field using electromagnetic conductivity imaging

J. Huang[a], E. Scudiero[b], H. Choo[a], D.L. Corwin[b], J. Triantafilis[a,*]

[a] School of Biological, Earth and Environmental Sciences, Faculty of Science, UNSW Australia, NSW 2052, Australia
[b] USDA-ARS, 450 West Big Springs Road, U.S. Salinity Laboratory, Riverside, 92507-4617 CA, USA

ARTICLE INFO

Article history:
Received 3 July 2015
Received in revised form 3 September 2015
Accepted 4 September 2015
Available online 26 October 2015

Keywords:
DUALEM-421
Soil volumetric water content
EM inversion
Water use efficiency

ABSTRACT

The ability to measure and map volumetric soil water (θ) quickly and accurately is important in irrigated agriculture. However, the traditional approach of using thermogravimetric moisture (*w*) and converting this to θ using measurements of bulk density (ρ—cm^3/cm^3) is laborious and time consuming. To speed up the process electromagnetic (EM) instruments have been used to assist in mapping average θ along a transect or across a field. This is because the apparent soil electrical conductivity (EC_a) measured by EM instruments has been shown to be a function of θ, when other soil properties are uniform. However, mapping depth-specific soil θ has been little explored. One possible approach is to invert the EC_a data to calculate estimates of true electrical conductivity (σ) at specific depths (i.e., 0.15, 0.45, 0.75, 1.05 and 1.35 m) and couple this to measured θ. This research explores this possibility by using a single frequency multi-coil DUALEM-421 across a centre-pivot irrigated Lucerne field (*Medicago sativa* L.) in San Jacinto, CA, USA. The first aim is to determine an optimal set of inversion parameters (i.e., forward modelling, inversion algorithm and damping factor—λ) which are appropriate to establish a calibration between σ and θ. In this regard the largest coefficient of determination ($R^2 = 0.56$) is achieved when we used the FS model, S2 algorithm and a $\lambda = 0.3$. The second aim is to see if all the coil arrays of the DUALEM-421 are necessary. We conclude that while the DUALEM-1 produces a larger R^2 (0.59), the use of the DUALEM-421 data is better ($R^2 = 0.56$), because the total model misfit (4.70 mSm^{-1}) is smaller and because it better accounts for the spatial variation of θ in the subsoil. In terms of predicting θ, the calibration equation ($\theta = 2.751 + 0.190 \times \sigma$) was examined using a leave-one-out cross validation. The Lin's concordance (0.73) between measured and predicted θ was good. The resulting 2-d depth slices and cross-sections gave insights into the spatial distribution of θ which allowed the inference of depth of saturated soil and location of the wetting front and identified areas where deep drainage may be problematic. The approach has applications for water use and management given it can identify inefficiencies in water application rates and use.

1. Introduction

Although it represents a small percentage (~0.05%) of globally available freshwater (Dingman, 2002), soil moisture is a key store of water in the hydrologic cycle and is of importance to hydropedological (Dunne et al., 1975), biological (Rodriguez-Iturbe, 2000) and biogeochemical processes (White et al., 1997). Of equal significance is that agriculture is the largest user with approximately 70% of water use (Fischer et al., 2007) with nearly 40% of food supply coming from irrigation (FAO, 2002). Because of the transient nature of soil moisture, it is crucial that it be measured, so that its variation can be quickly determined over large areas and at various depths. This information can subsequently be used for applying irrigation water variably under precision irrigation scheduling (Hedley et al., 2010). The most accurate method is to determine wetness (w—$g\,g^{-1}$), which is time consuming, because: (i) it requires 24 h oven drying during which time field conditions change (Blonquist et al., 2006), and (ii) measurements of bulk density (ρ—$cm^3\,cm^{-3}$) are necessary to enable estimation of volumetric moisture content (θ—$g\,cm^{-3}$).

To improve efficiency in measuring θ, several field instruments are commonly used, including time domain reflectometry (TDR) (Wraith et al., 2005) and neutron probes (Kodikara et al., 2013). Either way extrapolation over the field scale is difficult if soil type is unknown; given θ is influenced by texture and salinity. To improve efficiency in mapping θ, electromagnetic (EM) induction

* Corresponding author. Fax: +1 61 2 9385 1558.
E-mail address: j.triantafilis@unsw.edu.au (J. Triantafilis).

http://dx.doi.org/10.1016/j.agwat.2015.09.003
0378-3774/

instruments can be used (Huth and Poulton, 2007). This is because the measured soil apparent electrical conductivity (EC_a) is a function of θ, salinity, organic matter content, bulk density (ρ), and texture (Corwin et al., 2003). If these other factors remain constant, differences in θ can be measured and mapped. Kachanoski et al. (1988) first demonstrated this potential when they calibrated average (0.5 m) θ measured using a TDR to EM38 EC_a. Subsequent work by Kachanoski et al. (1990) confirmed these results using neutron probe measured average (1.7 m) θ. More recently, Hedley et al. (2013) mapped average (0.5 m) θ across an irrigated field using EM38 EC_a, whilst Robinson et al. (2009) mapped θ at a depth of 0.4 m with time and across a small catchment.

Although successful results have been achieved for estimating and mapping average θ and available water content (e.g., Gooley et al., 2014), few studies have mapped θ at different depths and as a function of EC_a. One way to do this is to use multiple (i) EM instruments of varying coil spacing (i.e., using EM38 and EM31) and/or (ii) coil orientations (i.e., vertical and horizontal) and coupled with inversion software. This would be akin to using direct current resistivity instruments and res2dinv software (GeoTom Software, 2010), which when used in concert have been useful in inferring θ variation at various depths in irrigated (Kelly et al., 2011) and dryland (Schwartz et al., 2008) systems. One reason the approach has not been explored for EC_a data has been the lack of easy-to-use software. However, recent research has demonstrated that EM4Soil can be used to jointly invert single frequency EM38 and EM31 EC_a to map salinity (Triantafilis and Monteiro Santos, 2009; Huang et al., 2015) or using a single frequency and multiple coil arrayed DUALEM-421 to map exchangeable sodium percentage (Huang et al., 2014) and clay (Triantafilis et al., 2013).

In this research we aim to determine the ability of DUALEM-421 EC_a to develop electromagnetic conductivity images (EMCIs) using EM4Soil software and to establish a single linear-regression (LR) between calculated true electrical conductivity (σ) and θ at various depths. The first task is to determine a suitable inversion algorithm (e.g., full solution), forward modelling (e.g., S1) and damping factor (e.g., λ = 0.3). We then assess whether all coil arrays of the DUALEM-421 are necessary to predict θ. In doing this we also simulate and demonstrate the usefulness of single coil array instruments (i.e., DUALEM-1 or EM38) as well as dual array configurations (i.e., EM38 and EM31 or DUALEM41). We also see how the use of additional arrays assesses the non-uniqueness issue. Once an optimal set of coil arrays is determined we test how well we can predict soil θ across an irrigated Lucerne field near San Jacinto. We chose this crop and field because a recent report by the U.S Global Change Program (Georgakakos et al., 2014) projects annual precipitation to decrease in southwest U.S.A, making water an increasingly valuable resource and because more than 40,000 ha of Lucerne is grown in California; making the crop the largest user of irrigation water due to the amount grown and its long growing season (Hansen et al., 2008).

2. Materials and methods

2.1. Study site

The study field is located on Scott Brothers' Dairy Farm in Southern California's Riverside County (lat. 33°50′25.43″N, long. 117°00′14.93″W) approximately 9 km northwest from downtown San Jacinto (Fig. 1). The study field is 32 ha and is farmed with irrigated Lucerne (*Medicago sativa* L.), which is used for consumption on-farm in a dairy feed lot. Since the 6th of March 2008, dairy lagoon water has been used. The average properties of the water (between March 2008 and June 2009), indicate that the pH is slightly alkaline (pH 7.8) and slightly saline (EC_{iw} = 1.63 dS/m). Given the SARw is 4.3 the potential for water infiltration problems is unlikely (Ayers and Westcot, 1994), however (Corwin et al., 2010).

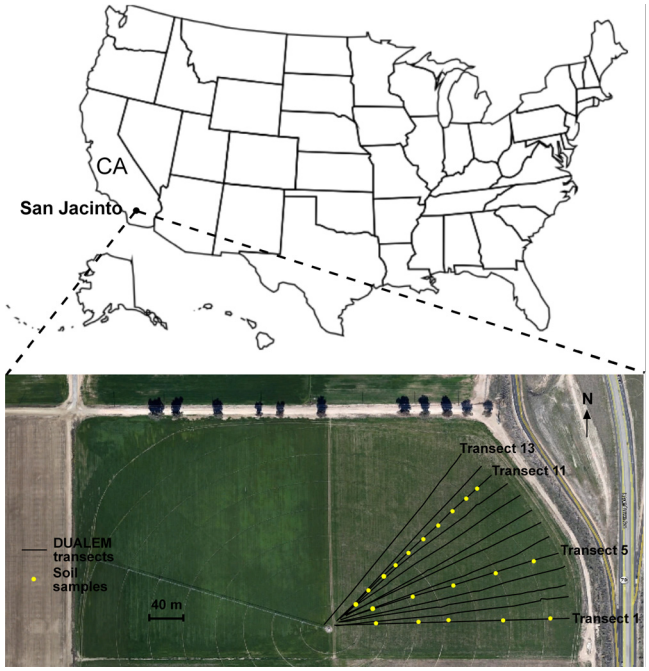

Fig. 1. Location of study area, EC_a transects and soil sampling locations on transects 1, 5 and 11.

2.2. DUALEM-421, data collection and interpolation

The DUALEM-421(DUALM Inc., Milton, ON, Canada) is a single-frequency (9.0 kHz) multi-coil arrayed (i.e., 6) EM instrument which operates at low induction numbers and consists of a transmitting coil (Tx) and three receiver coil (Rx) pairs. The Tx and one Rx pair have horizontal windings which form a horizontal coplanar array (HCP). The distances between the Tx to the coplanar Rx are 1, 2, and 4 m. The notation 1mHcon, 2mHcon, and 4mHcon represents EC_a and corresponds to measurements of approximately 0–1.5, 0–3.0, and 0–6.0 m, respectively. The other coils in each Rx pair have vertical windings and with the Tx forms perpendicular arrays (PRP). The distances between the Tx to the Rx are 1.1, 2.1, and 4.1 m, respectively. The respective EC_a measurements are represented by 1mPcon, 2mPcon, and 4mPcon with theoretical depth of corresponding to approximately 0–0.6, 0–1.2, and 0–2.4 m, respectively.

2.3. EC_a data, soil sampling and laboratory analysis

The field was irrigated on 28 August 2014. Immediately after this 13 transects (see Fig. 1) were traversed across the south-eastern quadrant with EC_a acquired with a DUALEM-421. The instrument was carried at a height of 0.2 m. Latitude and longitude was acquired via a Trimble Hurrican L1 antennae. The GPS and DUELAM-421 EC_a were logged using a Trimble GPS Pathfinder Pro Series Receiver.

To calibrate the inverted DUALEM-421 EC_a (i.e., σ), several calibration sites were selected. As shown in Fig. 1 these were located on three separate transects. On transects 1 and 5, 5 soil samples sites were selected. On transect 11, 10 sites were chosen. At all these sites, soil samples were collected at 0.3 m intervals to a depth of 1.5 m. Sampling was carried out on the same data the EC_a was acquired. All samples were sealed in plastic bags. In addition, undisturbed soil cores were obtained for bulk density determination (ρ—g cm^{-3}) but only along transect 5.

Laboratory analysis included determination of soil wetness (w) using the thermogravimetric method. Using average values of ρ acquired along transect 5 and at each depth (see Huang et al., 2016) the volumetric moisture (θ) was estimated; w (i.e., $\theta = w \times \rho$). The electrical conductivity of a saturated soil-paste extract (EC_e—dS m^{-1}) was also determined (U.S. Salinity Laboratory Staff, 1954) with laboratory analysis of particle size fractions (i.e., sand, silt and clay) assessed using a hydrometer. In both cases, the samples were first air-dried and ground to pass a 2-mm sieve.

2.4. Quasi-2D inversion of DUALEM-421 data

EM4Soil is a software package (EMTOMO, 2014) that inverts EC_a data acquired at low induction numbers. The algorithm is described by Monteiro Santos et al. (2010). The software generates electromagnetic conductivity images (EMCI) which are a matrix of calculated true electrical conductivity (σ) that is constrained by neighbouring sites. A number of parameters can be chosen (Triantafilis and Monteiro Santos, 2013), including, forward modelling and inversion algorithms as well as a damping factor (λ). We describe each in turn.

In forward modelling, forward calculations and derivatives consider the cumulative function (CF) or a full-solution (FS) model. The modelling is conducted using a 1-dimensional laterally constrained approach (Auken et al., 2002), where 2-dimensional smoothness constraints are imposed. The inversion algorithms are variations of Occam regularization and include algorithm S1 and S2. The latter constrains EMCI variation around a reference model and is smoother than S1.

A damping or smoothing factor (λ) is also required. We aimed to determine the optimal combination of inversion parameters (i.e., λ, S1 or S2, CF or FS) for the quasi-2D inversion of DUALEM-421EC_a and using data acquired along transects 1, 5 and 11. In terms of λ we set it from 0.07, 0.3, and 0.3 increments to a maximum of 3.0. Inversion of EC_a was generated with a maximum of 10 iterations. We calculated σ using a uniform initial model ($\sigma = 100$ mS m^{-1}).

2.5. EMCI modelling using EM4 soil

The main aim is to develop a calibration relationship between σ and θ and to map the latter in 2-d and across multiple transects. In the first instance we do this only along transect 11 where we have 50 soil samples to determine soil θ. We do this to identify a suitable set of EM4soil inversion parameters; whereby we vary the forward modelling (CF and FS), inversion algorithm (S1 and S2) and value of λ (e.g., 0.07, 0.3, 0.6, 1.2, 1.8, 2.4 and 3.0). By comparing the Pearson's correlation coefficient (Pearson's r), which describes the linear correlation between σ and θ, we select the EM4Soil parameters which achieves the maximum Pearson's r value.

To determine whether all 6 coil arrays are necessary we used these inversion parameters and varied the coil arrays available and to establish a calibration between σ and θ. In doing this our aim is to see if satisfactory results could still be achieved using a single pair of Rx or multiple pairs of Rx. The former reflects the idea of whether similar results could be achieved using only a DUALEM-1 (or EM38) while the latter indicates the usefulness of having multiple coil arrays such as a DUALEM-41 (equivalent to using EM38 and EM31). Linear regression modelling in all calibrations was performed using the Fit Model Tool available in JMP 10.2 (SAS Institute, 2012).

The use of varying the number of coil arrays is also aimed at understanding the problem of non-uniqueness; also known as the equivalence problem. The issue arises because for any given set of EC_a collected, any number of combinations of layers of different thicknesses and conductivity can give rise to the same response or measurement in EC_a (Keller and Frischknecht, 1966; Koefoed, 1979; Sharma and Kaikkonen, 1999). Several studies have been conducted to minimize this issue (Mester et al., 2011; Dafflon et al., 2013; von Hebel et al., 2014). We address this issue by comparing the results of linear regression modelling but also by calculating the misfit as follows:

$$\text{misfit} = \sqrt{\frac{1}{N}\sum_{i=1}^{N}(measured(EC_a)_i - \text{modelled}(EC_a)_i)^2}, \quad (1)$$

where N is the number of EC_a measurements, measured$(EC_a)_i$ and modelled$(EC_a)_i$ represent the ith measured EC_a and modelled EC_a values, respectively. The average misfit value for EC_a recorded with different coil arrays (e.g., 1mHcon and 1mPcon) is the total misfit.

2.6. Validation of prediction precision and bias

A linear regression model was used to establish a relationship between σ and θ using all the calibration data available on transects 1, 5 and 11. That is, 100 soil samples were available from the 20 calibration sites where samples were collected at 5 depth increments (e.g., 0–0.3, and 1.2–1.5 m). To evaluate prediction precision (root-mean-square-error, RMSE) and bias (mean error, ME) of the linear regression model, a leave-one-out cross-validation approach was used. Specifically, one sample is removed with the remaining 99 used to establish a linear regression relationship between σ and θ. This procedure was repeated until all the samples had been removed once.

3. Results and discussion

3.1. Distribution of EC_a and soil properties along transect 11

Fig. 2a shows 1mHcon and 1mPcon collected along transect 11. The 1mHcon (48.4 mS m^{-1}) is on average slightly higher than lmPcon (46.6 mS m^{-1}). Many of the local EC_a lows coincide with wheel tracks. Fig. 2b shows the 2mHcon and 2mPcon. Similar patterns in EC_a fluctuations are apparent, with 2mPcon slightly larger on average (51.2 mS m^{-1}) than 2mHcon (40.7 mS m^{-1}). This suggests a slightly larger conductor in the topsoil (0–0.3 m) and subsurface (0.3–0.6 m) than in the subsoil (>0.6 m). Fig. 2c shows the 4mHcon and 4mPcon. Average 4mHcon (38.1 mS m^{-1}) is also smaller than the average 4mPcon (48.1 mS m^{-1}).

Fig. 3a–c show the spatial distribution of measured clay, silt and sand, respectively. Fig. 3c indicates that texture in the topsoil (0–0.3 m) and subsurface (0.3–0.6 m) is mainly sandy loam except between sites 9 and 10 where it is loamy. The subsoil consists of a mix of sandy loams and loamy sands, the latter characterizing the area near the center pivot. Fig. 3d shows that topsoil EC_e is only slightly saline (2–4 dS m^{-1}), but progressively increases in the subsurface to moderately saline (4–8 dS m^{-1}) with EC_e strongly saline (>8 dS m^{-1}) at sites 4 and 8.

Fig. 3e shows the spatial distribution of volumetric water content (θ—cm^3 cm^{-3}). These were calculated using $w \times \rho$; where average values were used (see Huang et al., 2016). Furthest away from the center pivot and at site 9 topsoil and subsurface θ is intermediate-large (0.20–0.25 cm^3 cm^{-3}) and large (>0.25 cm^3 cm^{-3}). Given the loam texture this amount of water (0.20–0.30 cm^3 cm^{-3}) is indicative of θ close to field capacity (Allen et al., 1998). This is similarly the case with respect to the sandy loam textured soil (0.18–0.28 cm^3 cm^{-3}) that characterizes the topsoil and subsurface along the rest of the transect; where θ was intermediate (0.15–0.20 cm^3 cm^{-3}). The deeper subsoil (i.e., >0.9 m), however, is for the most part characterized by small θ (<0.10 cm^3 cm^{-3}). This value of θ is indicative of a loamy sand but at permanent wilting point (0.03–0.10 cm^3 cm^{-3}).

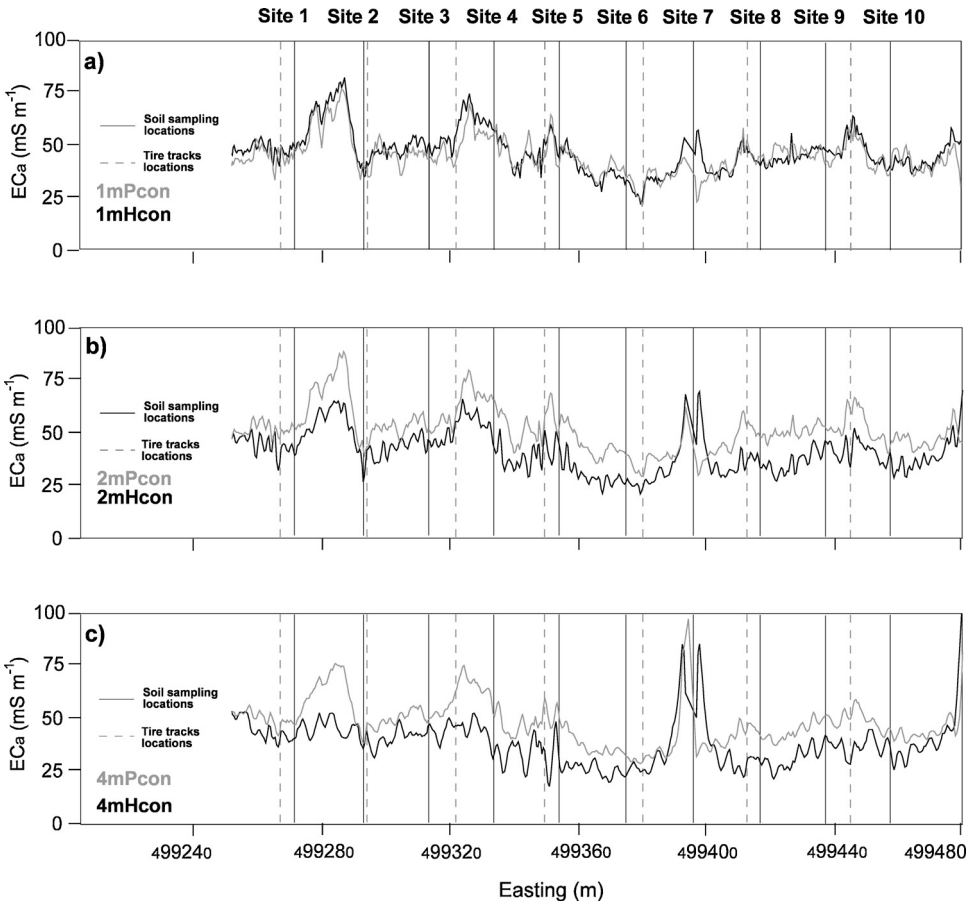

Fig. 2. Distribution of measured apparent soil electrical conductivity (EC_a—mS m^{-1}) by DUALEM-421 along the transect 11 and including; (a) 1mHcon and 1mPcon, (b) 2mHcon and 2mPcon, and (c) 4mHcon and 4mPcon.

3.2. Determining the optimal arrays of a DUALEM-421 for non-uniqueness problem

In order to determine a suitable set of EM4soil inversion parameters to estimate σ and to establish a linear regression with θ we generated a large number of EMCIs along transect 11 and by varying the model (CF and FS), algorithm (S1 and S2) and value of λ (e.g., 0.07, 0.3, 0.6,. . ., 3.0). We determined the largest Pearson's r (i.e., $r = 0.80$) was achieved when we used the FS model, S2 algorithm and $\lambda = 0.3$ (results not shown). The linear regression is of the form:

$$\theta = 2.751 + 0.190 \times \sigma. \quad (2)$$

In order to determine whether all 6 coil arrays are necessary we used these inversion parameters and varied the coil arrays available and to establish a calibration between σ and θ. In doing this our aim is to see if satisfactory results could still be achieved using a single pair of Rx or multiple pairs of Rx. Table 1 shows the summary statistics of the various regression models between σ and θ when inverting different coil arrays. In terms of the model misfit calculated by EM4Soil, the smallest misfit (i.e., 2.10 mS m^{-1}) was achieved using the DUALEM-4 EC_a. This is followed closely by the DUALEM-2 (2.21 mS m^{-1}) and DUALEM-21 (3.80 mS m^{-1}) EC_a. Interestingly, the DUALEM-1 produced the largest misfit (6.1 mS m^{-1}) followed by the DUALEM-41 EC_a (5.19 mS m^{-1}). A moderate misfit is produced by the DUALEM-421 (4.70 mS m^{-1}).

When comparing the coefficient of determination (R^2) between σ and θ, the strongest was achieved using a DUALEM-1 ($R^2 = 0.59$). This was followed closely by using all coil arrays of the DUALEM-421 ($R^2 = 0.56$). Dropping the 2 m Rx (i.e., DUALEM-41) led to a reduced coefficient ($R^2 = 0.55$). The poorest correlation was achieved using a DUALEM-4 ($R^2 = 0.30$). This result is interesting because the DUALEM-4 misfit was smallest as compared to the other coil array configurations. This was followed by the DUALEM-2 ($R^2 = 0.35$). Slightly better and moderate correlations were achieved using a DUALEM-21 ($R^2 = 0.41$) and DUALEM-42 ($R^2 = 0.43$).

To determine the correlation between measured and predicted θ (i.e., Lin's concordance), a leave-one-out cross validation approach indicated that the best result (0.75) was achieved by a DUALEM-1. This was again followed closely by a DUALEM-421 (0.75) and DUALEM-41 (0.71). The rank order of Lin's concordance for the other arrays was similar to the R^2. Similar results for RMSE and ME were also observed. To better appreciate these results we plot predicted θ with depth using the different DUALEM configurations.

3.3. 2-D modeling of θ using various coil arrays of the DUALEM-421

Fig. 4 shows the 2-d images of predicted θ along transect 11 from inverting EC_a of different configurations of the DUALEM. Fig. 4a shows θ using the DUALEM-421. While it is difficult to qualitatively compare predicted and measured θ; a few observations can be made. The first is predicted topsoil θ was intermediate-large (0.20–0.25 cm^3 cm^{-3}) and large (i.e., >0.25 cm^3 cm^{-3}) and reflects the large measured θ; which represent saturated topsoil conditions. The discrete and undulating nature of topsoil θ also indicates the location of the individual sprinklers.

In comparison, θ in the subsurface (0.3–0.6 m) is intermediate (0.15–0.20 cm^3 cm^{-3}) and decreases into the shallow subsoil (0.6–0.9 m) to intermediate-small (0.10–0.15 cm^3 cm^{-3}) values.

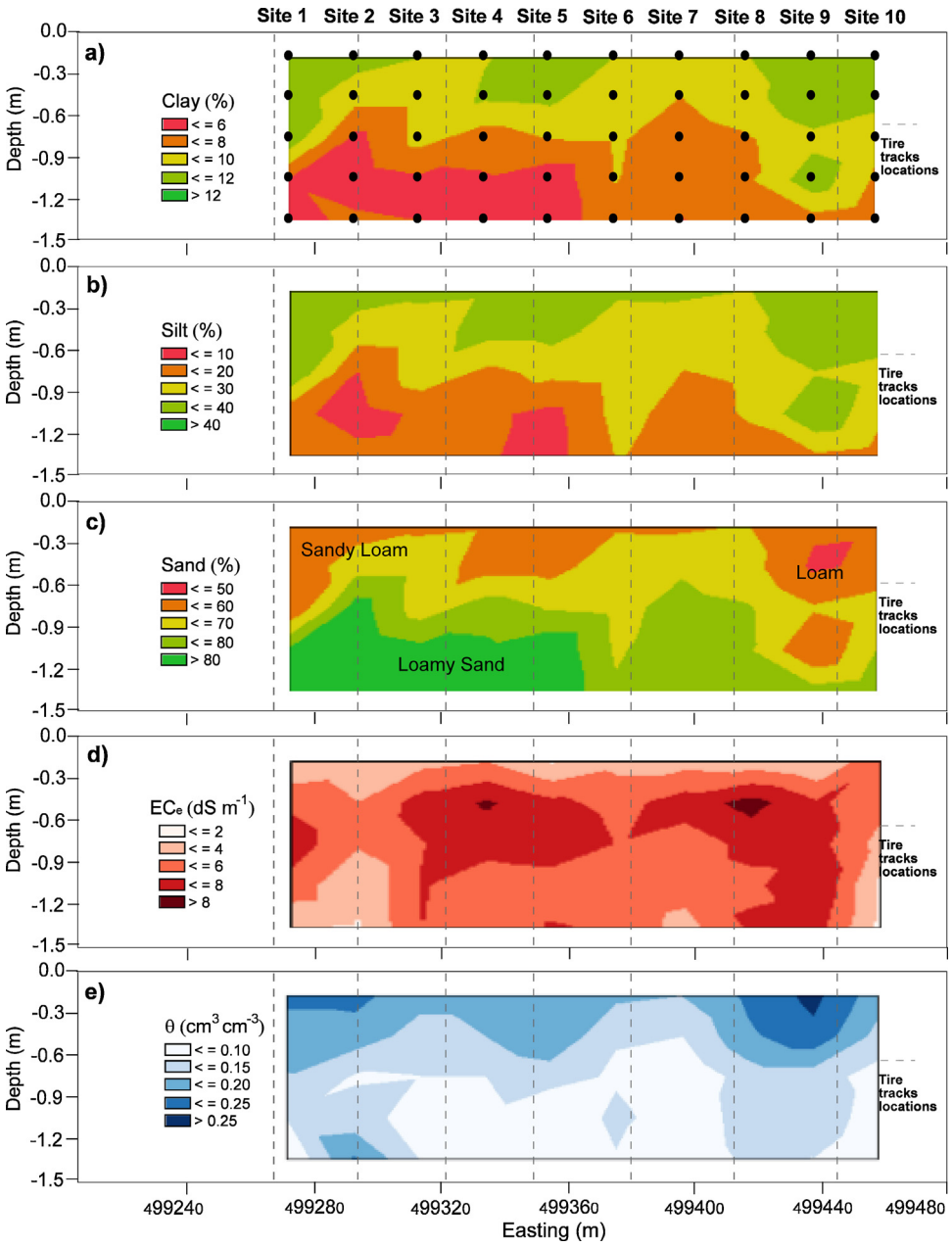

Fig. 3. Contour plots of various soil properties measured along transect 11 and including, (a) clay (%), (b) silt (%), (c) sand (%), (d) electrical conductivity of a saturated soil-paste extract (EC_e—dS m^{-1}), and (e) volumetric water content (θ—cm^3 cm^{-3}). Note: soil texture shown in part (c) was estimated using the USDA textural soil classification.

Table 1
Summary statistics of the various regression models.

DUALEM configurations	Model misfit (mS m^{-1})	Coefficient of determination (R^2)	Lin's concordance	RMSE (cm^3 cm^{-3})	ME (cm^3 cm^{-3})
421	4.70	0.564	0.726	0.036	0.000
1	6.12	0.590	0.747	0.035	−0.000
2	2.21	0.352	0.536	0.044	0.000
4	2.10	0.300	0.497	0.045	−0.000
41	5.19	0.548	0.713	0.036	−0.000
42	4.03	0.426	0.614	0.041	−0.000
21	3.80	0.405	0.587	0.042	0.000

The latter indicates the wetting front, given the smallest values (<0.10 cm^3 cm^{-3}) are indicative of loamy sands at permanent wilting point (Allen et al., 1998). In some instances, in particular those areas associated with tire tracks of the pivot irrigation gantry, predicted θ is small. We attribute this to soil compaction and reduced hydraulic conductivity and water entry. We also note that at either end, deep drainage appears to be being modelled and where the wetting front extends beyond 1.5 m.

Fig. 4b shows θ when we inverted the DUALEM-1 EC_a. This is equivalent to using an EM38 in horizontal and vertical modes.

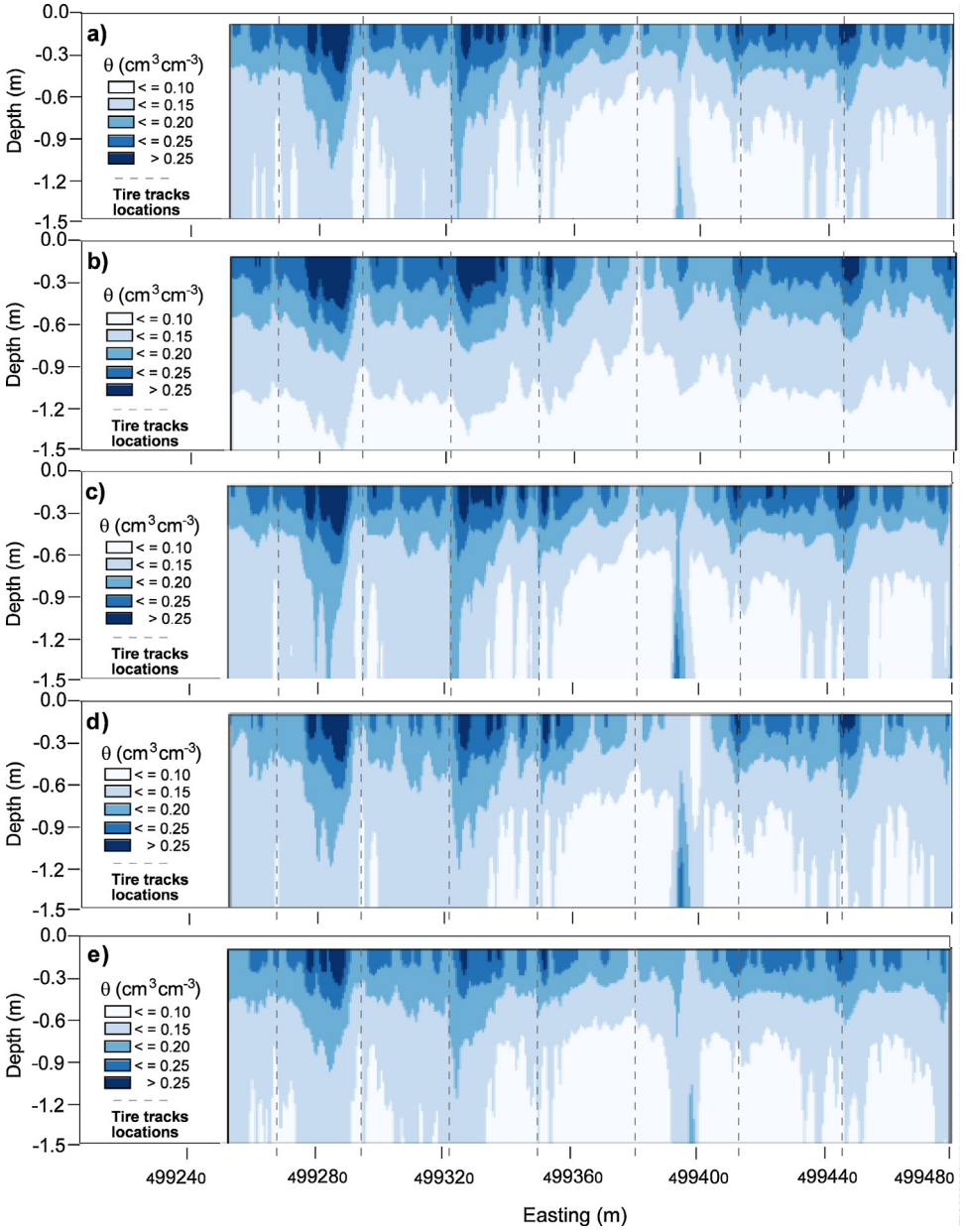

Fig. 4. Predicted volumetric water content (θ—$cm^3\ cm^{-3}$) from the inversion of bulk apparent electrical conductivity (EC_a—$mS\ m^{-1}$) collected using a (a) DUALEM-421, (b) DUALEM-1, (c) DUALEM-41, (d) DUALEM-42, and (e) DUALEM-21 and along transect 11.

Predicted topsoil and subsoil θ was similar to what was achieved using all coil arrays. The difference is that the wetting front appears much deeper (~1.2 m), particularly in the center.

Fig. 4c shows θ using inversion of DUALEM-41 EC_a. This configuration is equivalent to using two of the most popular Geonics EM instruments, namely an EM31 and EM38, in both modes of operation. By adding the 4 m Rx, subsoil θ appears to be better represented and more indicative of measured θ. Fig. 4d shows the result using a DUALEM-4. Here, and while subsoil θ is well represented and suggests deep drainage may be problematic at either end of transect 11, topsoil θ appears under predicted. We attribute the latter to the absence of the DUALEM-1 data.

Fig. 4e shows θ generated when data equivalent to a DUALEM-21. The model resembles that of the DUALEM-421 with subtle differences mainly occurring in the subsoil. This suggests that including DUALEM-4 data allows topsoil and subsoil to be modeled better.

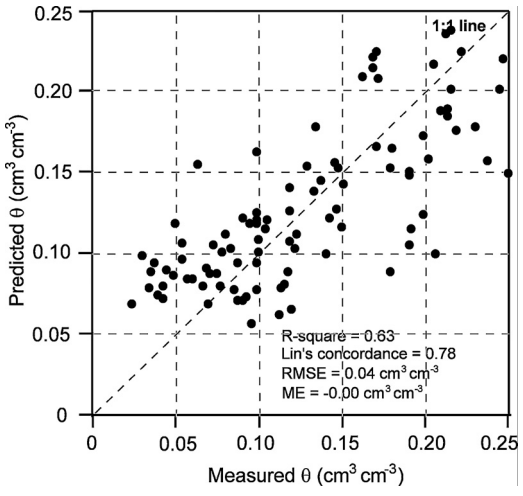

Fig. 5. Measured versus predicted soil volumetric water content (θ—$cm^3\ cm^{-3}$) generated by leave-one-out cross validation.

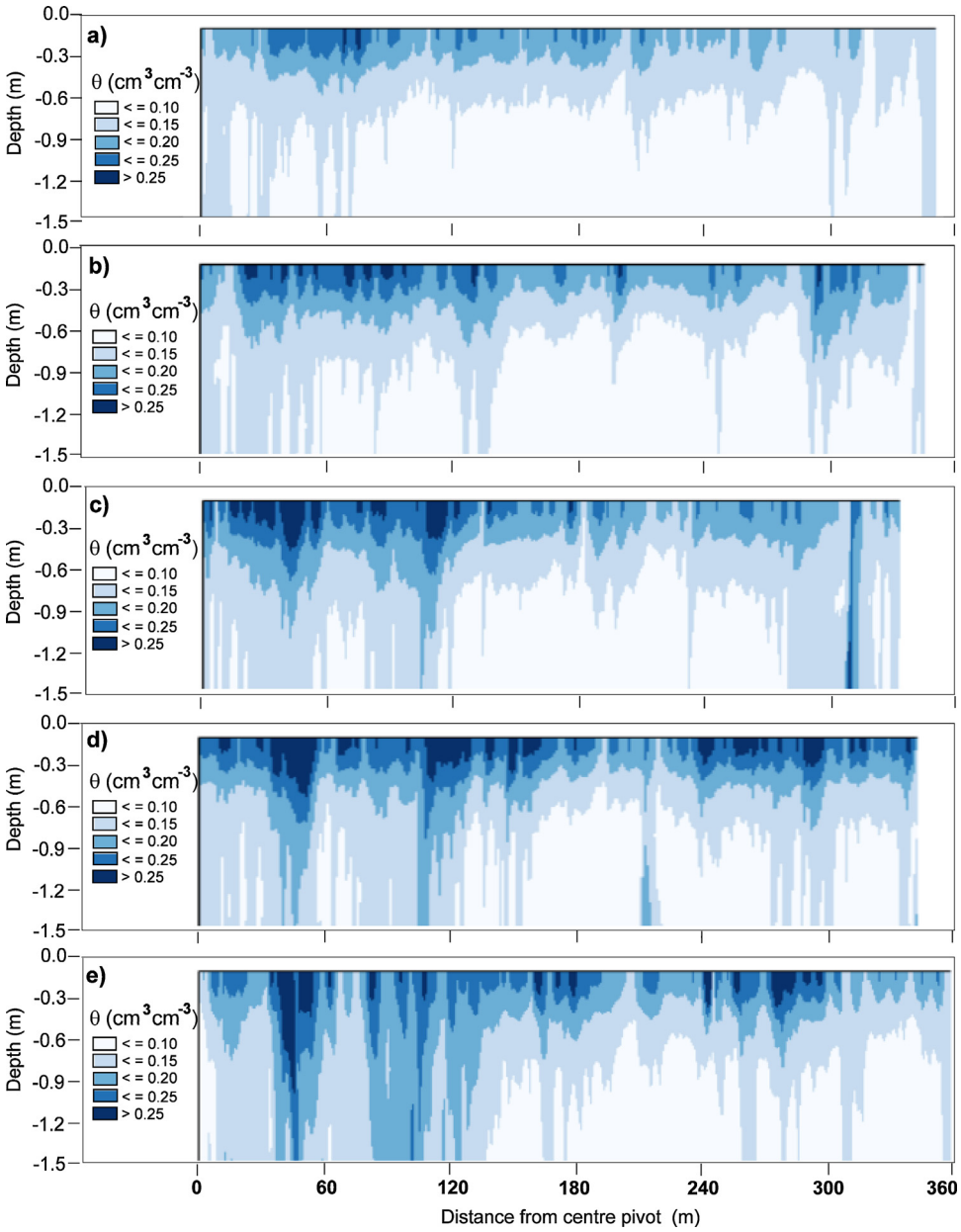

Fig. 6. Predicted volumetric water content (θ—$cm^3\ cm^{-3}$) from the inversion of bulk apparent electrical conductivity (EC_a—$mS\ m^{-1}$) collected using a DUALEM-421 and along transects (a) 1, (b) 3, (c) 7, (d) 11, and (e) 13.

It is apparent that predicting θ by inverting EC_a data of various arrays is possible. However, and whilst the images generated by the DUALEM-1 EC_a gave the best correlation coefficient ($R^2 = 0.59$) and was optimal in other measures, the model misfit was the largest ($6.12\ mS\ m^{-1}$). Whilst reasonable predictions in θ were made with the DUALEM-1 subsoil θ appeared to be poorly resolved. In this regard, the use of all available DUALEM-421 arrays better resolve subsoil θ, albeit that the R^2 (0.63) and Lin's concordance (0.74) were slightly smaller. Crucially, the model misfit was much smaller ($4.70\ mS\ m^{-1}$). This suggests that the use of more EC_a data reduces the problem of non-uniqueness given there is more data available and therefore fewer possible models of σ. As such, we progress this research by considering all arrays of the DUALEM-421 and to map θ.

3.4. Validation of predicted θ across multiple transects

Fig. 5 shows measured versus predicted θ; the latter generated from a leave-one-out sample out cross validation prediction of all 100 soil samples and available on transects 1, 5, and 11. The cross validation equation has a good R^2 (0.63) but more importantly a good Lin's concordance (0.78), and a small RMSE ($0.04\ cm^3\ cm^{-3}$) and ME ($-0.00\ cm^3\ cm^{-3}$). The RMSE shows that the accuracy of prediction is good, with the ME indicating unbiased estimates.

3.5. Horizontal and vertical depth slices of predicted θ across multiple transects

Fig. 6 shows the 2-d images of predicted θ along various selected transects. The various hydrological features described previously are evident in these cross-sections, namely the saturated top-soil ($\theta > 0.25\ cm^3\ cm^{-3}$) and the location of the wetting front ($\sim 0.10\ cm^3\ cm^{-3}$). It is also evident that transect 1 (Fig. 6a) is the least wet and transect 13 (Fig. 6e) is the wettest. This is particularly the case within 150 m of the center pivot. Here the fact that intermediate θ ($0.15–0.20\ cm^3\ cm^{-3}$) extends beyond the depth of sampling indicates that deep drainage is likely to be occurring.

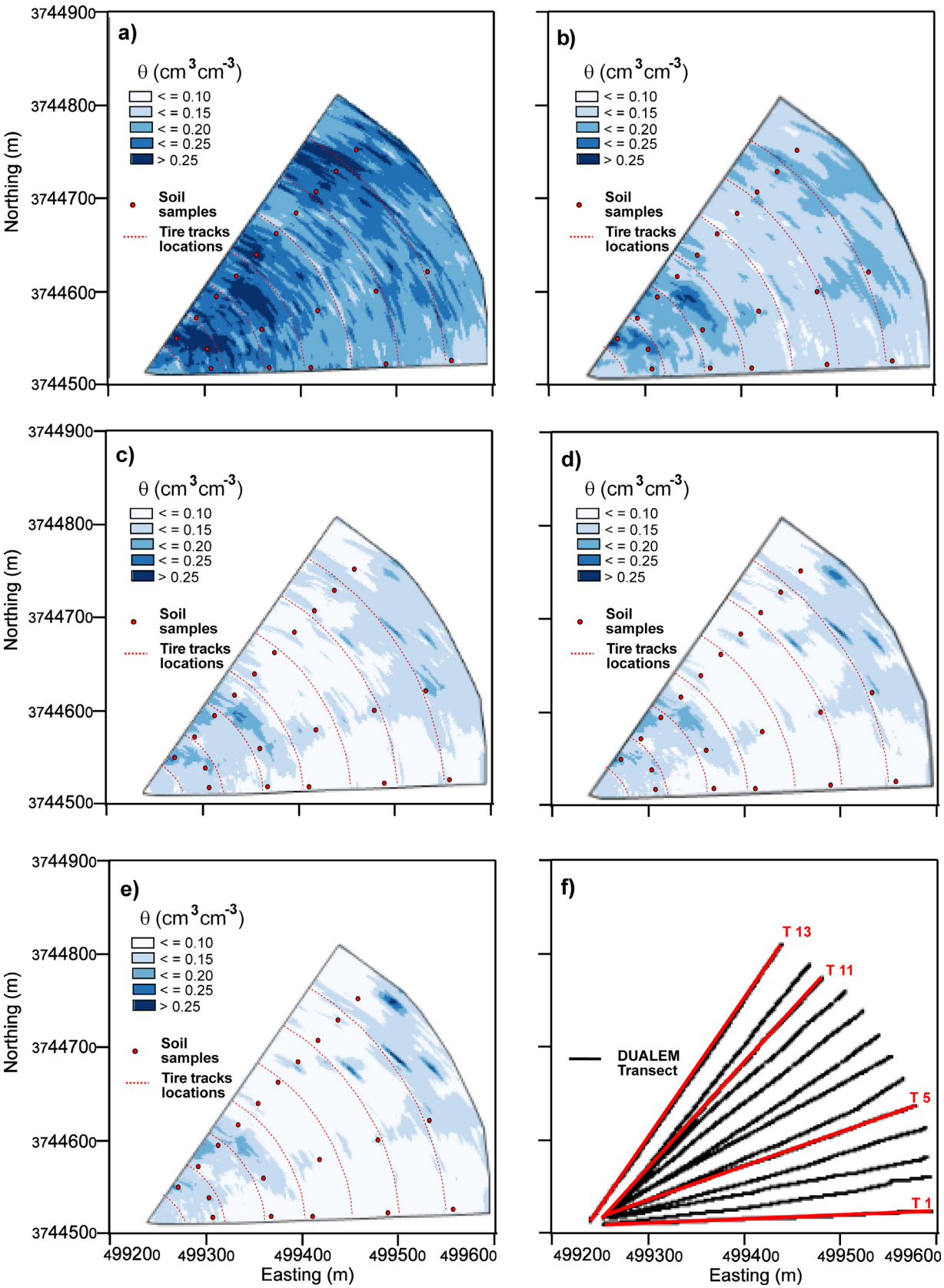

Fig. 7. Predicted volumetric water content (θ—$cm^3\ cm^{-3}$) from the inversion of bulk apparent electrical conductivity (EC_a—$mS\ m^{-1}$) collected using a DUALEM-421 and at various depth slices (a) 0–0.3, (b) 0.3–0.6, (c) 0.6–0.9, (d) 0.9–1.2, and (e) 1.2–1.5 m; and (f) location of DUALEM survey transects.

To better appreciate these results and place them in greater context we generated contour plots of predicted θ using all transect data. Fig. 7a and b show predicted θ in the topsoil and subsurface. In both cases the wettest areas ($\theta > 0.20\,cm^3\,cm^{-3}$) are within 150 m of the location of the center pivot. This is most likely because the sprinklers closer to the center pivot cover much less ground compared to those located furthest at the edge of the field; due to the shorter and longer arc of travel, respectively. As such, the part of the field closest to the pivot may be being over-irrigated, which is leading to saturated soil conditions, increased hydraulic conductivity and deep drainage and as suggested by the intermediate ($0.15–0.20\,cm^3\,cm^{-3}$) subsoil θ and shown in Fig. 7e.

Conversely, the smallest values of θ ($<0.10\,cm^3\,cm^{-3}$) are predicted in the southeast corner of the field and associated with transect 1. Here the soil is underlain by large amounts of gravel, which were encountered at a depth of around 0.9–1.2 m and along the entire transect at the time of sampling. This means the soil here drains freely. It is also worth noting the arc of small θ ($<0.10\,cm^3\,cm^{-3}$) in the center; coincident with the fifth and sixth tire tracks from the center pivot. This is most evident in the topsoil and subsurface depth slices (i.e., Fig. 7a and b, respectively). The reason is a function of soil compaction beneath the tire tracks and the higher bulk density. This was evident at the time of EC_a survey where the indentation of the tires was clearly visible on the soil surface. As a result infiltration is much reduced and predicted θ is small.

4. Conclusions

The development of EMCI across an irrigated Lucerne field and using a DUALEM-421 and easy to use EM4Soil inversion software has been shown to be a viable means of mapping θ at field scale with sufficient resolution and accuracy to assist site-specific irrigation management. This is the approach was able to resolve the effect of individual sprinklers and identify where the effect of the tire tracks was problematic. In addition, the inferences that were able to be made about the location of the wetting front and areas affected by deep drainage could be useful in improving irrigation management, particularly close to the close to the centre pivot.

At the present time, many examples are appearing in the literature about the use of DCR and GPR. We believe this approach overcomes many of the practical and operational issues which limit the applicability of these geophysical methods. Firstly, the non-contacting nature of EM means larger areas can be covered in shorter periods of time. Secondly, the single-frequency and multiple coil array of the DUALEM-421 enables different EC_a to be made at various depth increments and akin to variable electrode pairings of the DCR. The EM4Soil software allows inversion of this information to produce depth specific calculations of σ and the generation of EMCI which are akin to electrical resistivity images (ERI). The proximal nature of EM measurement is equivalent to that which can be achieved using a GPR but without the issues of single attenuation.

The success achieved herein was primarily a function of our decision to select a field (or part thereof) where soil texture and salinity profiles were, more or less, equivalent (Corwin and Lesch, 2013). This enabled us to establish a reasonable correlation between σ and θ. It was also because the variation in soil θ could be controlled given irrigation was conducted in the same way (i.e., sprinkler) and approximately the same rate and time. Future work could be directed at exploring the potential for developing a single calibration in a field of variable clay and EC_e. We also note that the approach is amenable for representing spatio-temporal change in θ, which was recently demonstrated by Huang et al. (2016) and along transect 5 in this field.

Acknowledgements

The authors acknowledge the numerous hours of diligent technical work performed in the field and the laboratory by Kevin Yemoto, Wes Clary and Michael Bagtang. We also thank Scott's Brothers Dairy Farm, particularly Bruce Scott, for allowing unrestricted access to their farm and field thus enabling us to undertake the research.

References

Allen, R.G., Pereira, L.S., Raes, D., Smith, M., 1998. Crop evapotranspiration. In: FAO Irrigation and Drainage Paper 56. Food and Agriculture Organization of the United Nations, Rome.

Auken, E., Foged, N., Sorensen, K.I., 2002. Model recognition by 1-D laterally constrained inversion of resistivity data. In: Matias, M.S., Grangeia, C. (Eds.), Proceedings of 8th Meeting Environmental and Engineering Geophysics, EEGS-ES. University of Aveiro Portugal, pp. 241–244.

Ayers, R.S., Westcot, D.W., 1994. Water Quality for Agriculture, Irrigation and Drainage Paper 29, Revision 1. Food and Agriculture Organization of the United Nations, Rome.

Blonquist, J., r, Jones, J.M., Robinson, S.B., DA, 2006. Precise irrigation scheduling for turfgrass using a subsurface electromagnetic soil moisture sensor. Agri. Water Manage. 84 (1), 153–165.

Corwin, D.L., Lesch, S.M., 2013. Protocols and guidelines for field-scale measurement of soil salinity distribution with EC_a-directed soil sampling. J. Environ. Eng. Geophys. 18 (1), 1–25.

Corwin, D.L., Lesch, S.M., Segal, E., Skaggs, T.H., Bradford, S.A., 2010. Comparison of sampling strategies for characterizing spatial variability with apparent soil electrical conductivity directed soil sampling. J. Environ. Eng. Geophys. 15 (3), 147–162.

Corwin, D.L., Kaffka, S.R., Hopmans, J.W., Mori, Y., Van Groenigen, J.W., Van Kessel, C., Lesch, S.M., Oster, J.D., 2003. Assessmentand field-scale mapping of soil quality properties of a saline-sodic soil. Geoderma 114 (3), 231–259.

Dafflon, B., Hubbard, S.S., Ulrich, C., Peterson, J.E., 2013. Electrical conductivity imaging of active layer and permafrost in an Arctic ecosystem, through advanced inversion of electromagnetic induction data. Vadose Zone J. 12 (4).

Dingman, S.L., 2002. Physical Hydrology, second ed. Prentice Hall, Upper Saddle River, N.J.

Dunne, T., Moore, T.R., Taylor, C.H., 1975. Recognition and prediction of runoff zones in humid regions. Hydrol. Sci. Bull. 20, 305–327.

EMTOMO, 2014. EM4Soil Version 2. EMTOMO, R. Alice Cruz 4, Odivelas, Lisboa, Portugal.

FAO, 2002. Food Balance Sheets. Food and Agricultural Organization of the United Nations. Rome.

Fischer, G., Tubiello, F.N., Van Velthuizen, H., Wiberg, D.A., 2007. Climate change impacts on irrigation water requirements: effects of mitigation, 1990–2080. Technol. Forecasting Social Change 74 (7), 1083–1107.

GeoTom Software, 2010. GeoTom LLC. 13,785 Diamond Path,Apple Valley, MN 55,124, USA.

Georgakakos, A.P., Yao, H., Georgakakos, K.P., 2014. Ensemble streamflow prediction adjustment for upstream water use and regulation. J. Hydrol. 519, 2952–2966.

Gooley, L., Huang, J., Page, D., Triantafilis, J., 2014. Digital soil mapping of available water content using proximal and remotely sensed data. Soil Use Manage. 30 (1), 139–151.

Hansen, J.R., Ernstsen, V., Refsgaard, J.C., Hansen, S., 2008. Field scale heterogeneity of redox conditions in till-upscaling to a catchment nitrate model. Hydrogeol. J. 16 (7), 1251–1266.

Hedley, C.B., Roudier, P., Yule, I.J., Ekanayake, J., Bradbury, S., 2013. Soil water status and water table depth modelling using electromagnetic surveys for precision irrigation scheduling. Geoderma 199, 22–29.

Hedley, C.B., Yule, I.J., Bradbury, S., 2010. Analysis of potential benefits of precision irrigationfor variable soils at five pastoral and arable production sites in New Zealand. In: 19th World Soil Congress, 1–6 August 2010, Brisbane, Australia: Proceedings DVD, ISBN: 978-0-646-53783-2.

Huang, J., Davies, G.B., Bowd, D., Monteiro Santos, F.A., Triantafilis, J., 2014. Spatial prediction of the exchangeable sodium percentage at multiple depths using electromagnetic inversion modelling. Soil Use Manage. 30 (2), 241–250.

Huang, J., Mokhtari, A.R., Cohen, D.R., Monteiro Santos, F.A., Triantafilis, J., 2015. Modelling soil salinity across a gilgai landscape by inversion of EM38 and EM 31 data. Eur. J. Soil Sci. 66 (5), 951–960.

Huang, J., Scudiero, E., Clary, W., Corwin, D.L., Triantafilis, J., 2016. Time-lapse monitoring of soil water content using electromagnetic conductivity imaging. Soil Use Manage., in press.

Huth, N.I., Poulton, P.L., 2007. An electromagnetic induction method for monitoring variation in soil moisture in agroforestry systems. Soil Res. 45 (1), 63–72.

Kachanoski, R.G., Wesenbeeck, I.V., Gregorich, E., 1988. Estimating spatial variations of soil water content using noncontacting electromagnetic inductive methods. Can. J. Soil Sci. 68 (4), 715–722.

Kachanoski, R.G., Wesenbeeck, I.V., Jong, E.D., 1990. Field scale patterns of soil water storage from non-contacting measurements of bulk electrical conductivity. Can. J. Soil Sci. 70 (3), 537–542.

Kelly, B.F.J., Acworth, R.I., Greve, A.K., 2011. Better placement of soil moisture point measurements guided by 2D resistivity tomography for improved irrigation scheduling. Soil Res. 49 (6), 661-669.
Keller, G.V., Frischknecht, F.C., 1966. Electrical methods in geophysical prospecting. International Series of Monographs in Electromagnetic Waves, 10.
Kodikara, J., Rajeev, P., Chan, D., Gallage, C., 2013. Soil moisture monitoring at the field scale using neutron probe. Can. Geotechol. J. 51 (3), 332–345.
Koefoed, O., 1979. Resistivity sounding on an earth model containing transition layers with linear change of resistivity with depth. Geophys. Prospect. 27 (4), 862–868.
Mester, A., van der Kruk, J., Zimmermann, E., Vereecken, H., 2011. Quantitative two-layer conductivity inversion of multi-configuration electromagnetic induction measurements. Vadose Zone J. 10 (4), 1319–1330.
Monteiro Santos, F.A., Triantafilis, J., Bruzgulis, K.E., Roe, J.A.E., 2010. Inversion of multiconfiguration electromagnetic (DUALEM-421) profiling data using a one-dimensional laterally constrained algorithm. Vadose Zone J. 9 (1), 117–125.
Robinson, D.A., Lebron, I., Kocar, B., Phan, K., Sampson, M., Crook, N., Fendorf, S., 2009. Time-lapse geophysical imaging of soil moisture dynamics in tropical deltaic soils: an aid to interpreting hydrological and geochemical processes. Water Resour. Res. 45 (4).
Rodriguez-Iturbe, I., 2000. Ecohydrology: a hydrologic perspective of climate-soil-vegetation dynamics. Water Resour. Res. 36 (1), 3–9.
Institute, S.A.S., 2012. JMP Version 10. SAS Institute Inc. Cary, North Carolina, USA.
Schwartz, B.F., Schreiber, M.A., Yan, T., 2008. Quantifying field-scale soil moisture using electrical resistivity imaging. J. Hydrol. 362, 234–246.
Sharma, S.P., Kaikkonen, P., 1999. Appraisal of equivalence and suppression problems in 1D EM and DC measurements using global optimization and joint inversion. Geophys.Prospect. 47 (2), 219–249.
Triantafilis, J., Monteiro Santos, F.A., 2013. Electromagnetic conductivity imaging (EMCI) of soil using a DUALEM-421 and inversion modelling software (EM4Soil). Geoderma 211–212, 28–38.
Triantafilis, J., Monteiro Santos, F.A., 2009. 2-dimensional soil and vadose zone representation using an EM38 and EM34 and a laterally constrained inversion model. Aust. J. Soil Res. 47 (8), 809–820.
Triantafilis, J., Terhune, C.H., Santos, F.M., 2013. An inversion approach to generate electromagnetic conductivity images from signal data. Environ. Modell. Softw. 43, 88–95.
Salinity Laboratory Staff, U.S., 1954. Diagnosis and improvement of saline and alkali soils. In: USDA Handbook 60. U.S. Government Printing Office, Washington, D.C., USA.
von Hebel, C., Rudolph, S., Mester, A., Huisman, J.A., Kumbhar, P., Vereecken, H., van der Kruk, J., 2014. Three-dimensional imaging of subsurface structural patterns using quantitative large-scale multiconfiguration electromagnetic induction data. Water Resour. Res. 50 (3), 2732–2748.
White, M.A., Thornton, P.E., Running, S.W., 1997. A continental phenology model for monitoring vegetation responses to interannual climatic variability. Global Biogeochem. Cycles 11 (2), 217–234, http://dx.doi.org/10.1029/97gb00330.
Wraith, J.M., Robinson, D.A., Jones, S.B., Long, D.S., 2005. Spatially characterizing apparent electrical conductivity and water content of surface soils with time domain reflectometry. Comput. Electron. Agric. 46 (1), 239–261.